

Article

Analysis of Electromagnetic Field Characteristics of Wave Glider

Taotao Xie , Jiawei Zhang , Dawei Xiao  and Qing Ji

College of Weaponry Engineering, Naval University of Engineering, Wuhan 430033, China;
xtt54321609@163.com (T.X.); david_engineer@126.com (D.X.); jiumingya886@163.com (Q.J.)

* Correspondence: gaweizhang@163.com; Tel.: +86-131-0065-0604

Abstract: A wave glider is an ocean observation platform that utilizes wave energy to drive and solar energy to power. Its metal structure will generate related electromagnetic fields due to corrosion and underwater motion. In the detection of weak electromagnetic field signals underwater, its own electromagnetic field characteristics will have an impact on signal detection. To study the applicability of electric field sensors and magnetic field sensors on wave glider platforms, the structural characteristics of the wave glider were analyzed, and the installation positions of electric field sensors and magnetic field sensors were designed based on the different motion states of the water surface mother body and underwater towing body. The measured electromagnetic field data of the wave glider platform were measured, and the measured data were analyzed. It was determined that the interference electric field energy under typical working conditions of the wave glider was mainly concentrated within 1 Hz, which decreased with increasing frequency, and the magnitude was mV/m. The magnitude of the interference magnetic field is several tens of nT, indicating that the electromagnetic field interference is significant during the working state of the wave glider. Installing an electric field sensor directly at the bottom of the wave glider will cause significant noise interference, while installing the magnetic field sensor directly at the bottom of the tractor will affect the servo and the shaking-induced magnetic field. Moreover, wave gliders should not use electric field signals below 1 Hz as signal sources, but they can utilize axial frequency electromagnetic fields to detect weak electromagnetic signals underwater.



Citation: Xie, T.; Zhang, J.; Xiao, D.; Ji, Q. Analysis of Electromagnetic Field Characteristics of Wave Glider. *Appl. Sci.* **2024**, *14*, 4800. <https://doi.org/10.3390/app14114800>

Academic Editors: Douglas O'Shaughnessy and Zaopeng Dong

Received: 12 April 2024

Revised: 28 May 2024

Accepted: 30 May 2024

Published: 1 June 2024



Copyright: © 2024 by the authors. Licensee MDPI, Basel, Switzerland. This article is an open access article distributed under the terms and conditions of the Creative Commons Attribution (CC BY) license (<https://creativecommons.org/licenses/by/4.0/>).

Keywords: wave glider; underwater electromagnetic field; target detection; applicability research; electromagnetic characteristic analysis

1. Introduction

Underwater unmanned systems can perform various tasks such as ocean exploration, underwater monitoring, reconnaissance, anti-mine and anti-submarine operations, and have high civilian and military value. They have gradually assumed important roles in underwater mining, hydrological collection, and other fields. At the same time, underwater unmanned systems have also become important pieces of supporting equipment for major military countries around the world to expand their underwater combat areas and occupy advantages in maritime operations [1,2]. At present, countries around the world attach great importance to the development of marine resources. There has been a growing interest in the exploration and oceanographic investigation of marine resources, and underwater attack and defense combat systems are facing enormous pressure. Unmanned equipment, represented by unmanned underwater vehicles, plays an increasingly important role in the future exploration of underwater resources and underwater confrontation [3–5].

As a new type of underwater observation platform that converts wave energy into motion energy, wave gliders rely on their own structural characteristics to achieve continuous detection of the underwater environment under different sea conditions, and because of their advantages in the field of observation, a variety of wave gliders equipped with various types of sensors have been used in related fields.

Currently, a large number of studies on path planning for wave gliders have been conducted in academia. The methods used in reference [6] include the weight-heuristic A* algorithm and WAPF algorithm, and in order to ensure the efficient navigation of wave gliders in complex marine environments and to maintain their controllability in upwind or downwind conditions, a hybrid path planning method aiming at path time consumption and safety was proposed. Meanwhile, Fen Liu et al. [7] investigated the interference and nonlinear effects caused by the interaction between the propeller and rudder in a wave glider with a special double-body structure and a higher maneuverability propeller-rudder control system. They proposed an improved adaptive model predictive control based on model predictive control, which can adaptively adjust the size of the prediction interval and the weight value of the rudder and the propeller according to the heading requirements. References [8,9] and others have studied the operation of wave gliders under different working conditions and formation conditions, and it is known that wave gliders have perfect working performance.

For the field of underwater detection using wave gliders, Surui Xie [10] designed measurement trajectories and found that the GNSS-a based on wave gliders can provide centimeter-level horizontal positioning accuracy for a single transmitter in shallow water, even if the sound speed model differs from the actual value by a few meters per second, making low-cost GNSS-A surveys in shallow water areas a promising reality. Zhilin Lyu [11] proposed a real-time ship detection system based on the YOLOv5s lite CBAM model, equipped with a visual detection and recognition system using a wave glider. A lightweight YOLOv5s lite CBAM model was proposed, which was embedded in the Jetson nano-A02 development board to achieve long-term recognition and monitoring of ships at sea in low-power mode, making the application of wave gliders in automatic coastal patrol more promising.

The authors of [12–15] developed a low noise detection system for passive acoustic monitoring of marine mammals by using a wave glider equipped with a low-power towed hydrophone array and an embedded digital signal processor. Reference [16] used a wave glider equipped with temperature and salinity depth sensors for observing surface water temperature and wave height in coastal locations with a flow velocity of approximately 0.5–1 m/s and a water depth of approximately 30–40 m.

It can be seen that underwater gliders equipped with sensors for ocean target detection have become a research hotspot in various countries. Underwater electromagnetic fields have the advantages of being less affected by hydrological and meteorological conditions, stable detection performance, and good concealment [17,18]. They have also been widely used in underwater target detection, recognition, and positioning [19–21].

The use of electricity and magnetic fields to detect underwater target signals needs to be based on accurate measurements. In terms of ocean electric field measurement, carbon fiber electrodes and Ag/AgCl electrodes are mainly used as electric field sensors, with Ag/AgCl electrodes being the most commonly used. Flux gate sensors are usually used to measure weak magnetic signals underwater. Electromagnetic sensors are sensitive to shaking due to their structural characteristics. Currently, there are no electromagnetic sensors installed on wave gliders. For underwater unstable platforms such as wave gliders, studying the electromagnetic field characteristics of wave gliders has practical engineering significance for the next step of underwater electromagnetic field detection.

The manuscript analyzes the structural characteristics and motion features of wave gliders, combines the practical application requirements of wave gliders equipped with electric and magnetic field sensors for underwater electromagnetic field detection, designs the wave glider platform installed with electric and magnetic field sensors, and carries out sea tests in a sea area of Qingdao, and tests and analyzes the electromagnetic field characteristics of the wave glider platform. Based on the sea test data, the electromagnetic self-noise of the platform is obtained, the noise characteristics of the platform are provided, and an engineering proposal for equipping underwater electromagnetic field sensors is put forward.

2. Analysis of Motion Characteristics of Wave Glider

A wave glider is a new type of unmanned mobile platform at sea that uses wave energy as the drive force and solar energy as the power source to overcome the bottleneck of energy supply for small underwater sports platforms. Wave gliders have the advantages of long sailing time, long sailing distance, low maintenance cost, suitability for high sea conditions, simple deployment and recovery, no dependence on chemical fuels, and small radar reflection area [22,23]. Wave gliders have significant research and practical value in both military and civilian applications [24]. For example, as a new type of mobile observation platform in civilian applications, they can be equipped with multiple sensors for research on marine meteorology, resource exploration, marine environment, and marine life. In the field of military defense, they can be used for communication relay, target reconnaissance, etc. [25].

Structure and Motion Characteristics of Wave Gliders

The wave glider studied in this manuscript is shown in Figure 1, and is mainly divided into two parts: a surface mother ship and an underwater towing machine, with a distance of 7 m between the two parts. The surface mother ship consists of a sealed cabin surrounded by solar panels, floating materials, a control system, a battery, various sensor loads, and rechargeable batteries. The glider consists of a rotatable wing panel, a wing panel support frame, and a steering engine. The upper part in contact with water is non-metallic, the underwater towing machine is made of stainless-steel, and the propeller blades of the towing machine are made of carbon fiber.

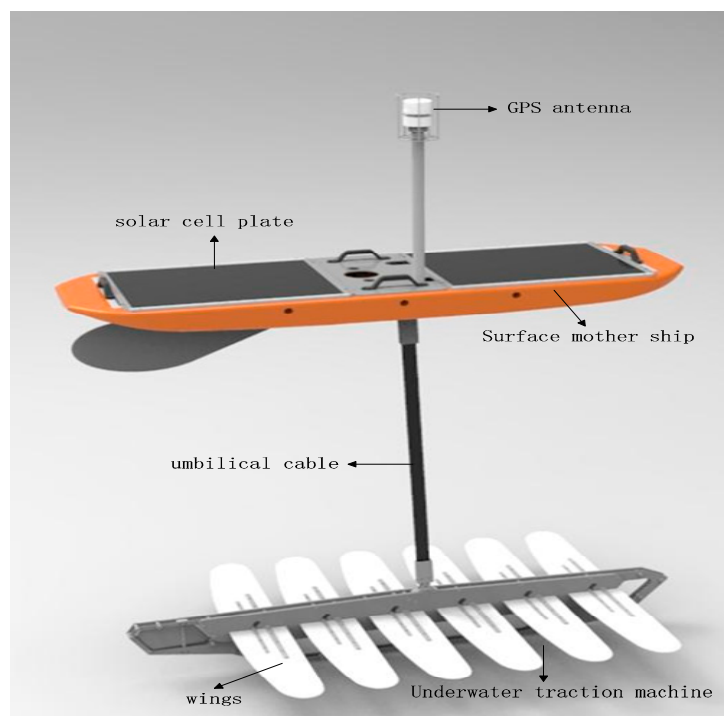


Figure 1. Schematic diagram of wave glider structure.

The wave glider relies on the mechanical energy of wave motion to convert it into forward thrust and maintain its motion characteristics. During its motion, the water wings on the wave glider rotate clockwise when descending and counterclockwise when ascending, generating hydrodynamic forces from the relative motion between the water wings and the ocean, thereby driving the underwater glider forward without being affected by the direction of the waves. The wave energy propulsion system is purely mechanical, and the propulsion device neither generates nor consumes electrical energy. The wave glider

has functions such as automatic navigation, position-keeping, and satellite communication monitoring. The platform is equipped with a satellite communication module, which can achieve real-time communication with the shore station and provide a continuous power supply to the load.

During the motion of a wave glider, when the floating body on the water surface undergoes a heave motion under the action of waves, the flexible connecting cable is affected by the combined force of the surface mother body and the underwater towing body. The underwater glider also generates a heave through the umbilical cable, so it is in two states of tension and relaxation. As the waves rise on the surface of the ship, the flexible cables are tensioned, and the underwater towing machine moves upward and forward under the pulling force of the surface ship. When the surface of the ship descends with the waves, the flexible cables relax, and the underwater towing machine dives under its own gravity and glides forward under the push of the wing plates. (The underwater glider studied in this manuscript is shown in Figure 2).

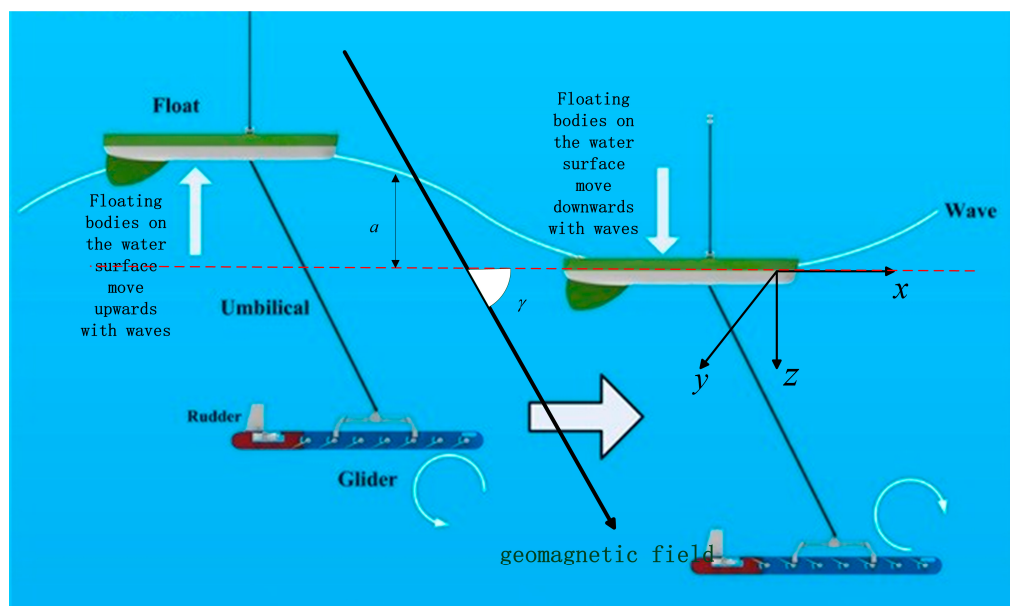


Figure 2. Principles of wave glider motion. The white arrow indicates the direction of movement, a indicates fluctuation amplitude.

The wave glider has a powerful and flexible sensor carrying capacity. For the detection of underwater electromagnetic targets, it can be known from its structure and motion characteristics that the floating equipment of the wave glider floats on the water surface. Therefore, the underwater electromagnetic detection equipment is not suitable to be installed on the floating body of the water surface, and its movement relies on the movement of waves, resulting in significant noise generated by shaking; therefore, considering the installation of electric field sensors on underwater traction machines, there will be two aspects of electric field interference. First, the traction machine will induce an electric field. As the traction machine is made of bare stainless-steel material (excluding blades), the working depth of the traction machine is 7 m. During the tensioning and loosening process of the connecting cable, shaking-related electric field noise will be generated; the second is the electromagnetic field generated by the rotation of the steering engine. In order to maintain the heading, the steering engine will continuously adjust the rudder angle underwater, resulting in electromagnetic field interference.

As shown in Figure 2, assuming the wave glider is moving along the x direction, the amplitude of its waves is a , the magnetic inclination angle of the geomagnetic field F is γ , and the angle between the glider's movement direction and the magnetic north is θ . i, j, k is defined as the unit vector in the x, y, z axis direction.

The geomagnetic field is a stable magnetic field, and its three components at the moving position are expressed as:

$$\mathbf{F} = F[(\cos \gamma \cos \theta)\mathbf{i} - (\cos \gamma \sin \theta)\mathbf{j} + (\sin \gamma)\mathbf{k}] \quad (1)$$

Assuming the glider's motion speed is:

$$\mathbf{V} = -a\omega(\mathbf{i} \cdot \mathbf{i} + \mathbf{k}) \exp(i\omega t - irx - rz) \quad (2)$$

In the formula, ω is the angular frequency; r is the angular wave number, $r = \omega^2/g$, where g is the gravitational acceleration; $i^2 = -1$.

The attitude change of a wave glider is a slow process, and the azimuth angle change is very small in the short term. Therefore, the angle between the measured electrode direction and the magnetic north pole can be regarded as a constant value in the short term. To simplify the calculation, assuming that the x -axis direction of the electric field is consistent with the direction of motion, there is a correlation between α_2 and the velocity v_x along the x -axis direction and the vertical velocity v_z , which can be expressed as follows:

$$\alpha_2(k) = f(v_x, v_z) = \sum_{n=0}^{N-1} [c_n v_x(k-n) + c'_n v_z(k-n)] \quad (3)$$

In the formula: k represents the discrete time; c_n , c'_n is α_2 and v_x , respectively. The coefficient between v_z ; N is the duration that needs to be accumulated.

According to Maxwell's law of electromagnetic induction, the three components of the electric field $\mathbf{E} = -\mathbf{V} \times (\mathbf{F} + \mathbf{H})$ can be obtained, where \mathbf{H} is the wave-induced magnetic field. Since $\mathbf{F} \gg \mathbf{H}$, this equation can be simplified as follows:

$$\mathbf{E} = -\mathbf{V} \times \mathbf{F} \quad (4)$$

3. Analysis of Electric Field Noise Characteristics

3.1. Installation Design of Electric Field Sensors

To avoid direct contact between the electric field sensors and the stainless-steel traction machine, a wooden board is added between the electric field sensor and the stainless steel to provide isolation and support. The electric field sensor uses a typical Ag/AgCl sensor, with the underwater traction body keel direction as the horizontal direction. The electric field sensor is divided into horizontal and vertical directions, and two sensors are installed in each direction. The electric field collection and storage device is installed at the head of the traction machine to reduce the impact of the collection device on the movement of the underwater traction body. The specific installation structure is shown in Figure 3.



Figure 3. Installation diagram of electric field sensor.

The experiment was conducted at a dock in Qingdao. Due to the depth of seawater at the experimental site being over 2 m, and considering that the height of the underwater towing body is about 30 cm, in order to ensure that the underwater towing machine and electric field sensor do not touch the bottom, the connecting cable between the surface mother ship of the wave glider and the underwater towing machine was shrunk to a length of about 1.2 m, which means that the working depth of the electric field sensor is about 1.5 m.

3.2. Simulation of the Motion State of a Wave Glider

The connecting cables between the surface floating body and the underwater towing body of the wave glider are in tension and relaxation states, and there are different motion states between the surface floating body and the underwater gliding body under the two different states. To analyze the electric field characteristics of the wave glider under different motion states, a crane was used to fix the wave glider in the experiment to control the depth of entry into the water. The bow and stern ends of the surface floating body were connected by towing ropes, and its motion direction was controlled to simulate the motion state of the wave glider's surface floating body, as shown in Figure 4.

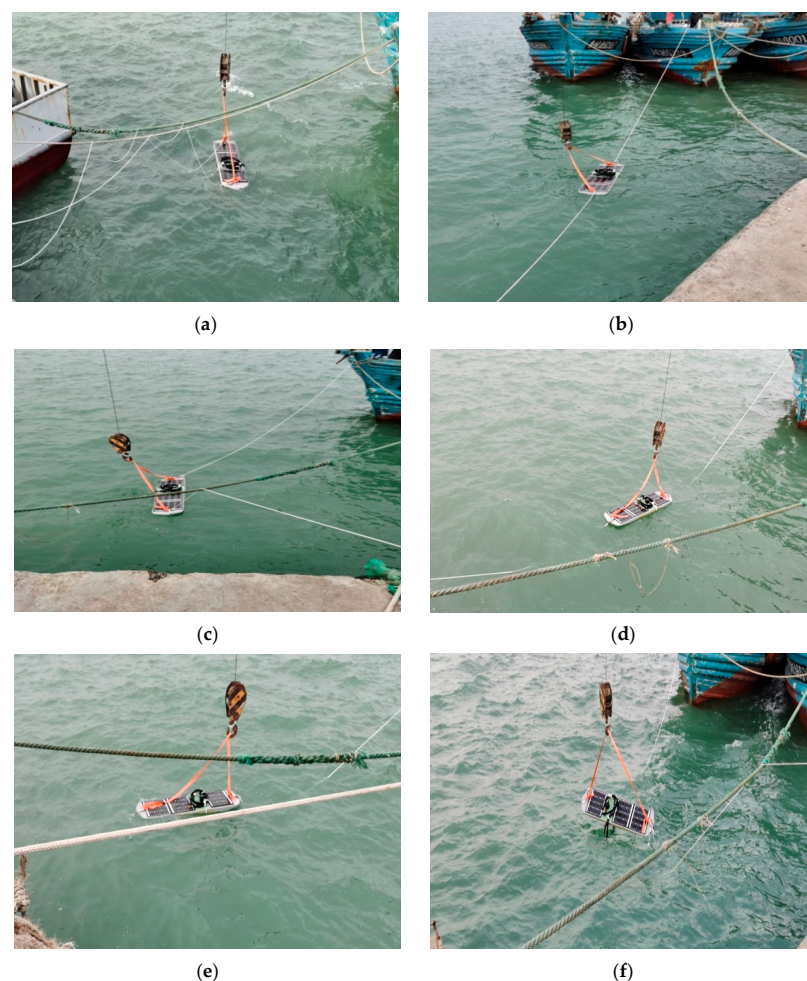


Figure 4. Simulation of the motion state of a wave glider. (a) Tensioning the suspension rope, the traction rope is not under force, and the floating body on the water surface is in a semi-free state. (b) The suspension rope is loose, the traction rope is tensioned, and the floating body on the water surface shakes parallel to the dock. (c) The suspension rope is loose, the traction rope is tensioned, and the floating body on the water surface shakes perpendicular to the dock. (d) Loose suspension rope, loose traction rope, and floating body on the water surface shaking parallel to the dock. (e) Loose suspension rope, loose traction rope, and floating body on the water surface shaking perpendicular to the dock. (f) Floating body on the water surface leaving the water.

As shown in Figure 4, the motion states (b), (c), (d), and (e) simulate the free movement of a floating body on the water surface. As a control group, by tightening the suspension rope on the surface of the floating body, (a) and (f) simulate the floating body in a semi-in-water and out-of-water state, control the relative motion between the surface floating body and the underwater towing body, and analyze the impact of the underwater towing body's rudder operation on the analysis of the electromagnetic characteristics.

3.3. Analysis of Electric Field Characteristics under Different Motion States

(1) Motion state (a)

As shown in Figure 5, the tow rope above the floating body on the surface of the water is under tension and in a semi-submerged state. At this time, the peak value of the electrostatic field is about 0.3 mV/m, and the peak value of the axial frequency electric field is about 0.2 mV/m. According to the power spectral density, it can be seen that the energy of the interference electric field is mainly concentrated at 1 Hz. During the measurement, there were large ships docked in the harbor, so it is reasonable that the degree of wave shaking was relatively small. The working period of the rudder of the underwater towing body is about 2 s, and according to the analysis of the power spectral density of the axial-frequency electric field, it can be seen that at this time the rudder in the towing body is working normally, and the interference electric field generated is larger.

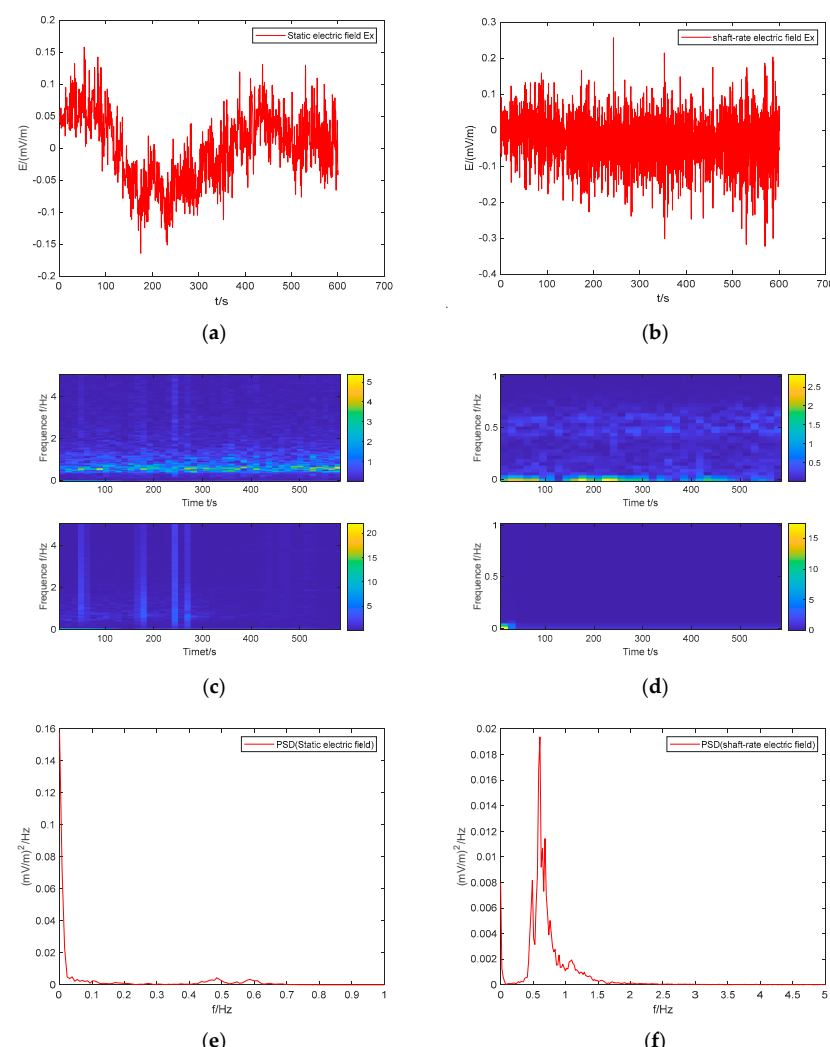


Figure 5. Analysis of electric field characteristics. (a) electrostatic field; (b) shaft-rate electric field; (c) time frequency diagram of electrostatic field; (d) time frequency diagram of shaft-rate electric field; (e) power spectral density of electrostatic field; (f) power spectral density of shaft-rate electric field.

(2) Motion state (b)

As shown in Figure 6, the surface float enters the water and is parallel to the direction of the pier. Through the tow rope to control the floating body swaying, the peak value of the electrostatic field was measured at about 0.25 mV/m, and the peak value of the axial frequency electric field was about 0.4 mV/m. According to the power spectral density, it can be seen that the energy of the electrostatic field is mainly concentrated in the 0.4–0.7 Hz range, and the energy of the axial frequency electric field is mainly concentrated in the 0.5–1 Hz range. At the time of measurement, large ships were leaving the harbor, and the waves in the harbor were fluctuating, resulting in a large increase in the measured interference electric field signal.

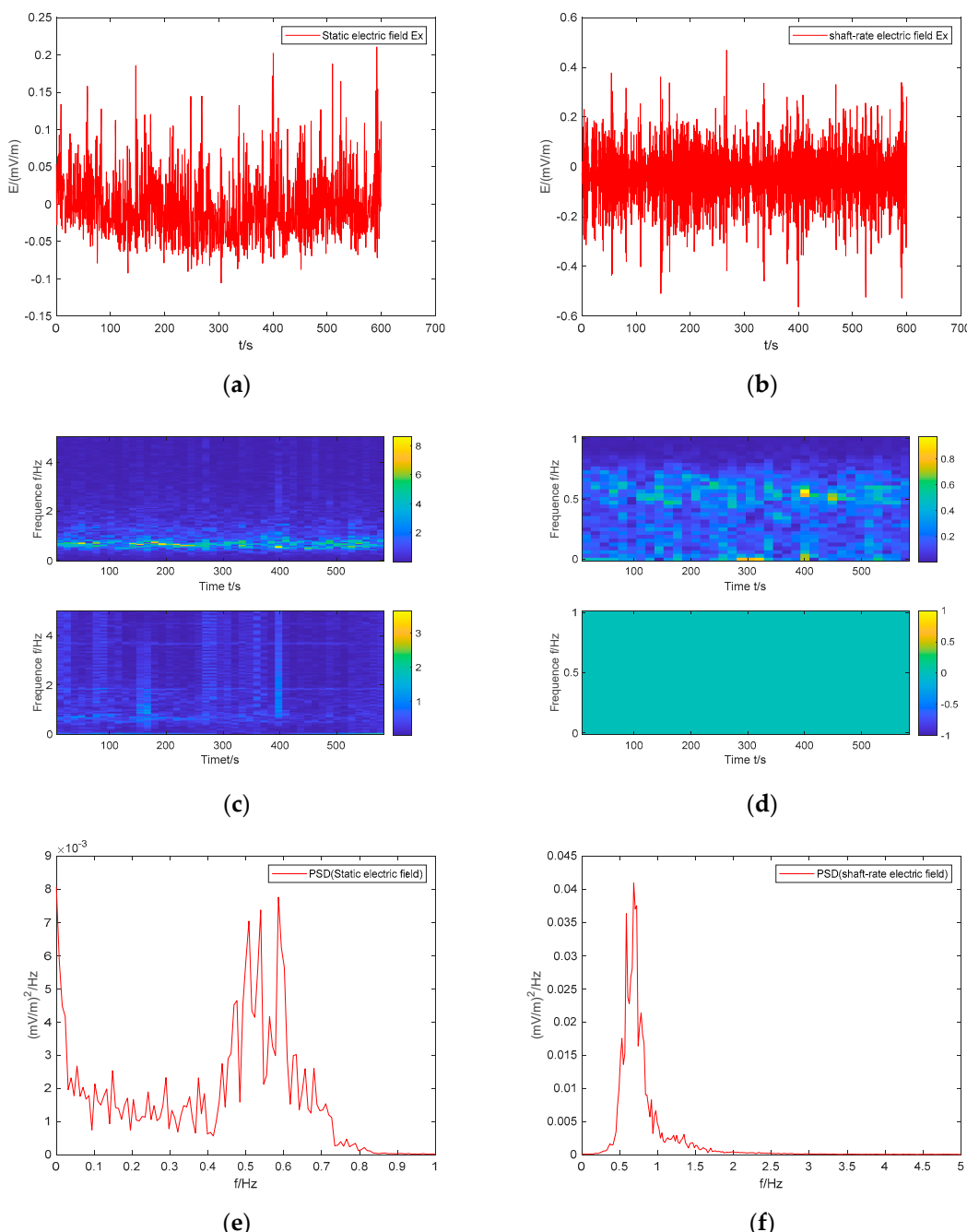


Figure 6. Analysis of electric field characteristics. (a) Electrostatic field; (b) shaft-rate electric field; (c) time frequency diagram of electrostatic field; (d) time frequency diagram of shaft-rate electric field; (e) power spectral density of electrostatic field; (f) power spectral density of shaft-rate electric field.

(3) Motion state (c)

As can be seen in Figure 7, at this point the surface float enters the water and is perpendicular to the dock. At this time, the surface floating body swaying is controlled by the tow rope. The peak value of the measured electrostatic field is about 0.25 mV/m, and the peak value of the axial frequency electric field is about 0.6 mV/m. Comparing with Figure 6, it can be seen that when the mother body is perpendicular to the dock, the peak value of the axial frequency electric field has a significant trend of increasing. Combining this observation with the analysis of the power spectral density of the axial frequency electric field, we observe that the energy is mainly concentrated in the 0.5–1.5 Hz range. This suggests that during the time when the submerged towing body is perpendicular to the dock, significant adjustments are required, resulting in greater rudder azimuth adjustments.

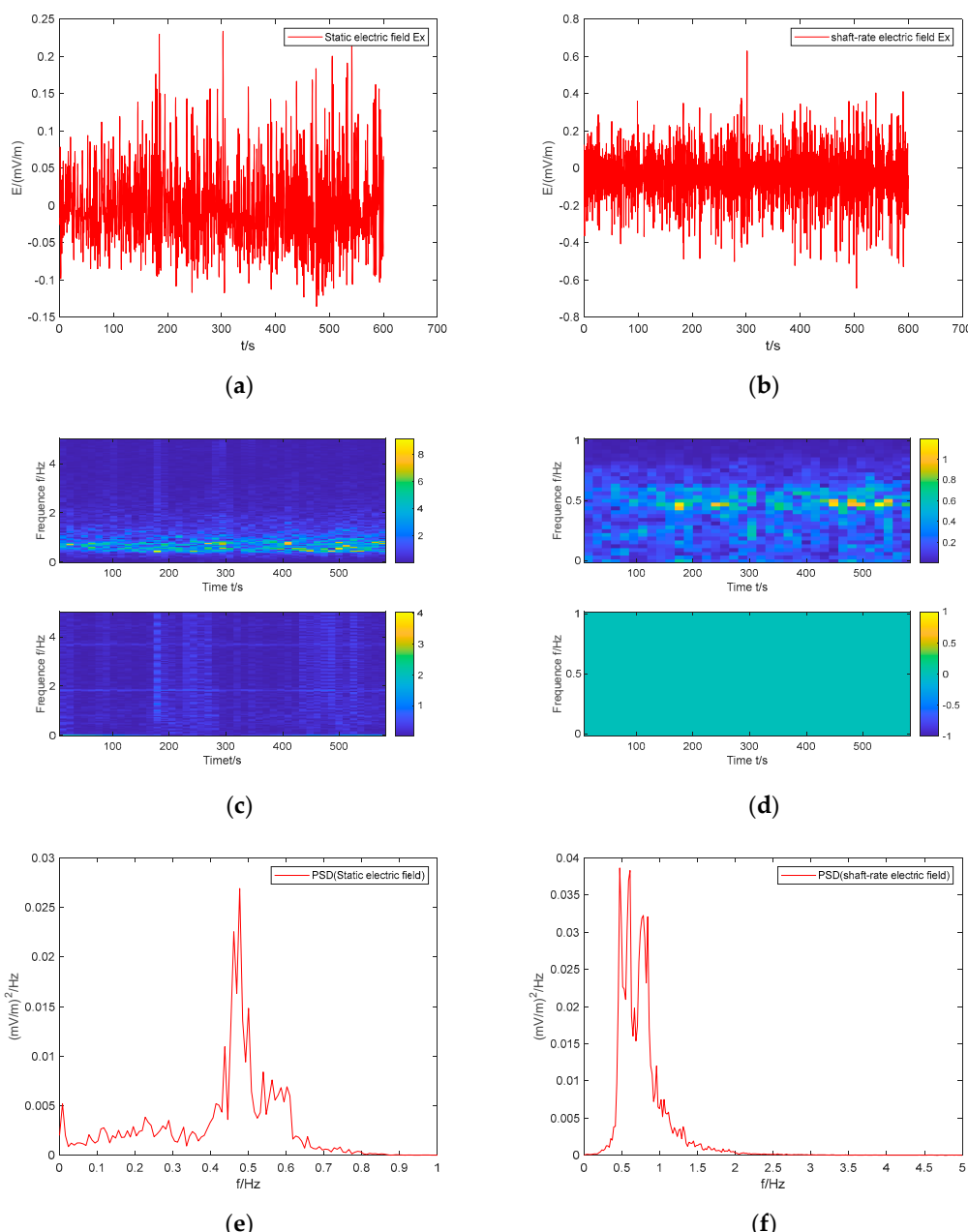


Figure 7. Analysis of electric field characteristics. (a) Electrostatic field; (b) shaft-rate electric field; (c) time frequency diagram of electrostatic field; (d) time frequency diagram of shaft-rate electric field; (e) power spectral density of electrostatic field; (f) power spectral density of shaft-rate electric field.

(4) Motion state (d)

As can be seen in Figure 8, the surface floating body is still parallel to the dock. At this time, the tow rope directly controls the swaying of the underwater tractor, so the swaying amplitude of the tractor increases. The peak value of the electrostatic field is about 0.35 mV/m, and the peak value of the axial frequency electric field is about 1 mV/m. The increase in the traction body swaying directly leads to the significant increase in the interference electric field signal; by analyzing the power spectral density, it can be seen that the traction body swaying also leads to the increase in the adjustment angle of the underwater rudder, which makes the axial frequency electric field signal increase.

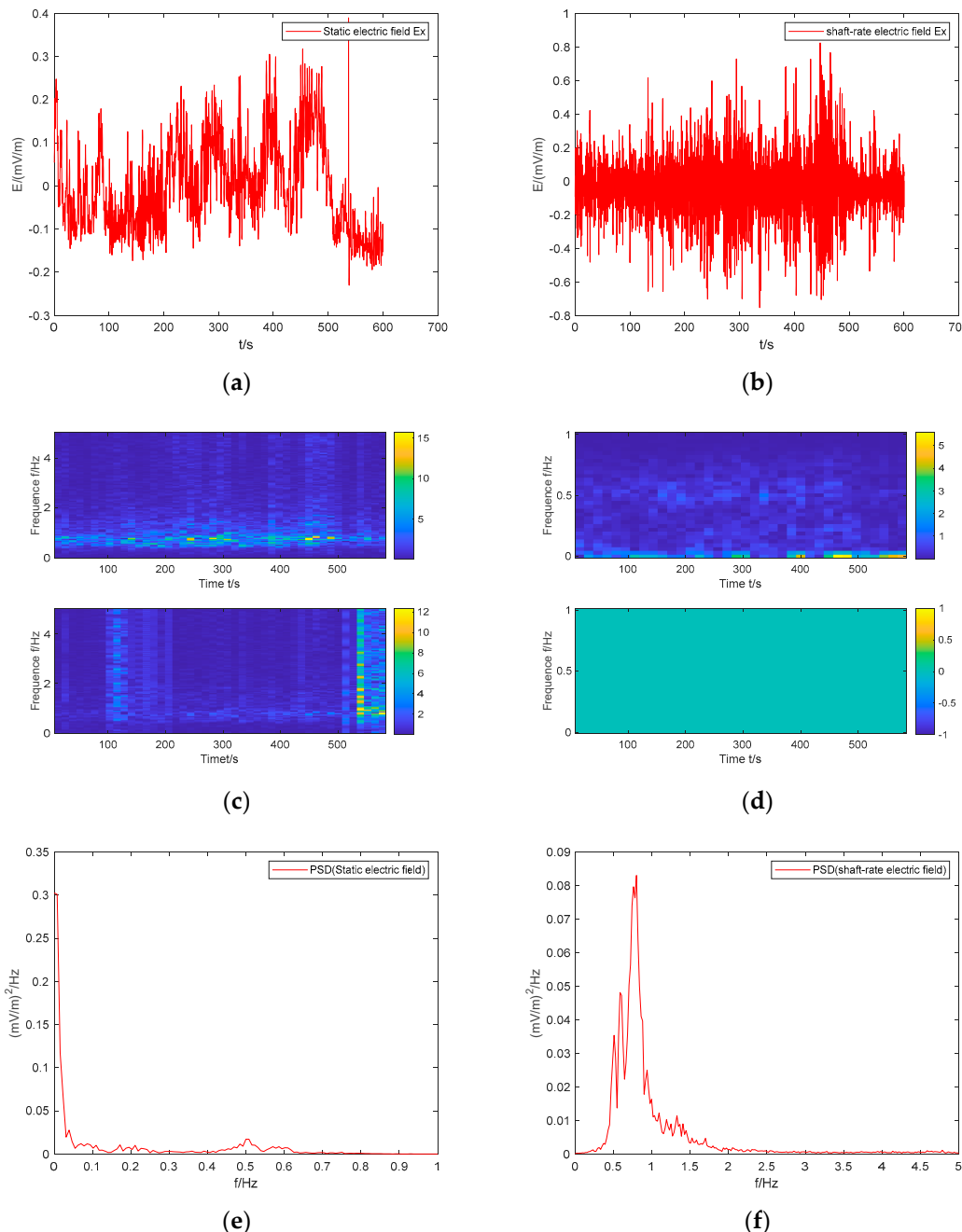


Figure 8. Analysis of electric field characteristics. (a) Electrostatic field; (b) shaft-rate electric field; (c) time frequency diagram of electrostatic field; (d) time frequency diagram of shaft-rate electric field; (e) power spectral density of electrostatic field; (f) power spectral density of shaft-rate electric field.

(5) Motion state (e)

As shown in Figure 9, the floating body on the water surface enters the water but is perpendicular to the dock. At this time, the traction rope of the underwater towing body is not under force, and the shaking amplitude of the towing body decreases. The peak value of the electrostatic field is about 0.30 mV/m, and the peak value of the axial frequency electric field is about 0.8 mV/m. Compared to Figure 9, the reduction in axial frequency electric field signal is relatively small. It can be seen that when the floating body on the water surface is perpendicular to the dock, the azimuth angle changes greatly, and the working amplitude of the servo is large, resulting in a larger axial frequency electric field signal.

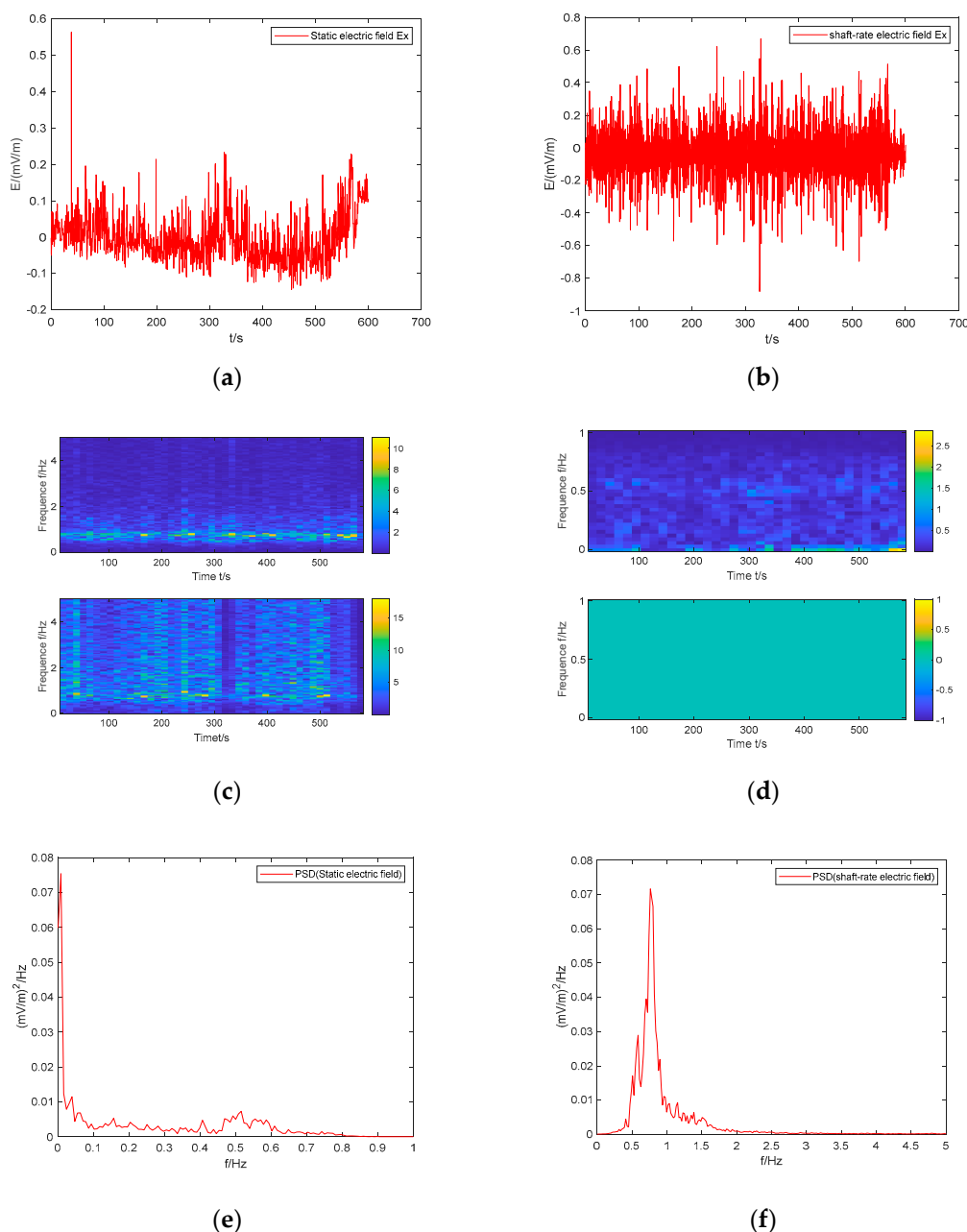


Figure 9. Analysis of electric field characteristics. (a) Electrostatic field; (b) shaft-rate electric field; (c) time frequency diagram of electrostatic field; (d) time frequency diagram of shaft-rate electric field; (e) power spectral density of electrostatic field; (f) power spectral density of shaft-rate electric field.

(6) Motion state (f)

As shown in Figure 10, the floating body on the water surface is lifted off the water surface by a crane. At this time, only the underwater towing body is working underwater, and the shaking of the towing machine is small. The motion state can be regarded as a stable state with only the underwater servo working. At this time, the peak value of the electrostatic field is about 0.10 mV/m, and the peak value of the axial frequency electric field is about 0.2 mV/m.

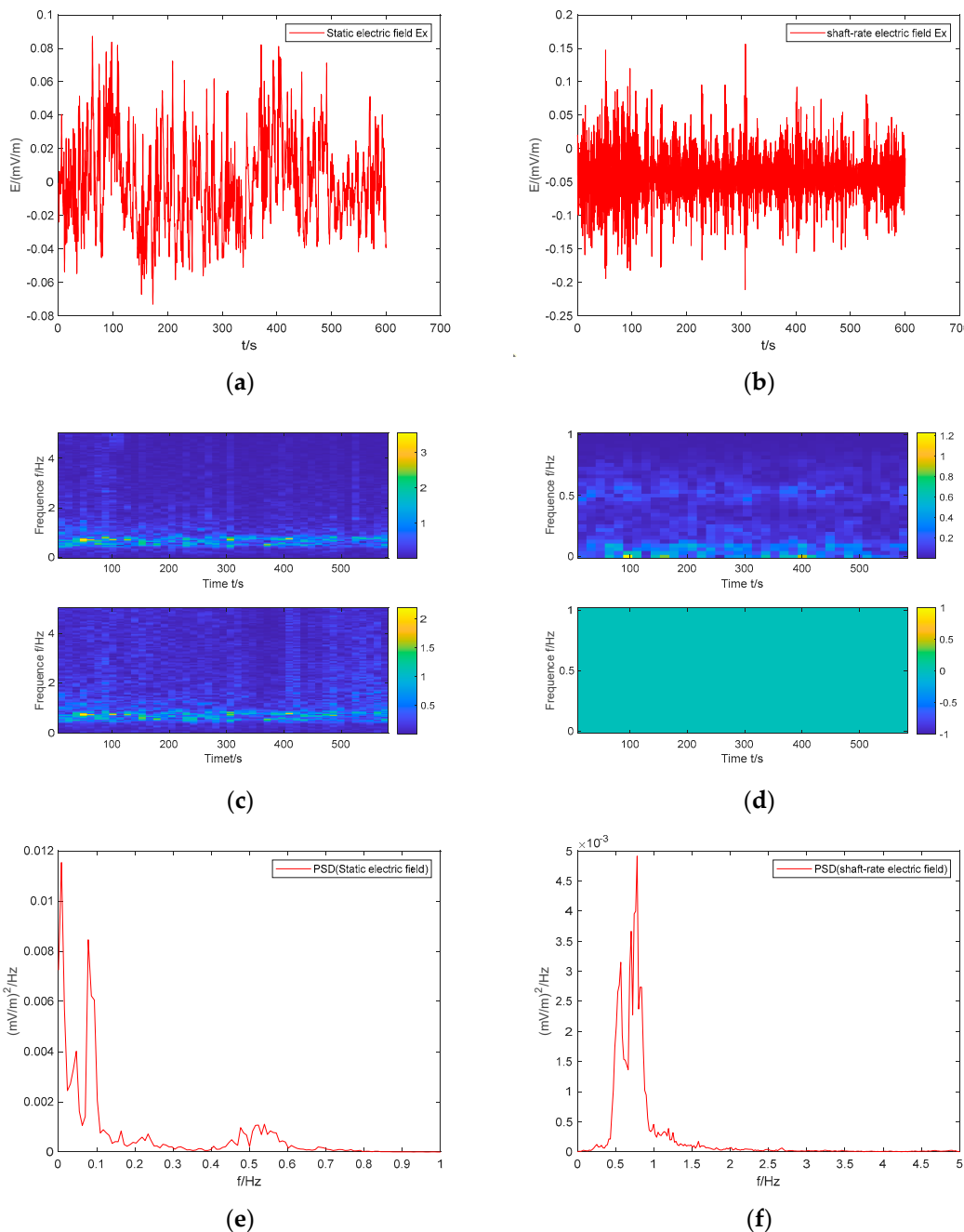


Figure 10. Analysis of electric field characteristics. (a) Electrostatic field; (b) shaft-rate electric field; (c) time frequency diagram of electrostatic field; (d) time frequency diagram of shaft-rate electric field; (e) power spectral density of electrostatic field; (f) power spectral density of shaft-rate electric field.

In the following paragraphs, we will summarize the electric field characteristics of wave gliders under different motion states.

By comparing Figures 5 and 10, it can be seen that when the mother ship leaves the water surface, the amplitude of the underwater towing body shaking decreases, and the electrostatic field generated by shaking is greatly reduced. However, the amplitude of the electric field generated by the operation of the towing body servo does not change much. By comparing Figures 6–9, it can be seen that the amplitude of the floating body's shaking on the water surface has a relatively small impact on the electrostatic field, while the amplitude of the underwater towed body's shaking has a more significant impact on the electrostatic field. By analyzing the working mechanism of the underwater towed rudder, it can be concluded that when it is perpendicular to the dock, the azimuth angle changes more as compared to when the floating body is parallel to the dock, resulting in a larger amplitude of rudder variation and a higher amplitude of axial frequency electric field.

By analyzing the motion state and combining it with data analysis, the following conclusions can be drawn:

- (1) In the range of 0.5~1 Hz, electric field interference is mainly generated by the steering engine (the action cycle of the steering engine is about 2 s). Comparing states 2–3, 4–5, and 6, it can be seen that the greater the shaking degree, the more obvious the steering engine action, and the greater the electric field interference;
- (2) According to Table 1, the peak-to-peak value of the axial frequency electric field is about 0.5~0.7 mV/m. At a depth of 50 m, the peak-to-peak value of the electric field in the same frequency band of the electromagnetic buoy is about 0.0001 mV/m. It can be seen that installing an electric field sensor directly at the bottom of the wave glider at this depth (<2 m) will cause significant noise interference, and the detection performance will be significantly reduced;
- (3) The peak value of the electrostatic field at the bottom of the glider is about 0.2~0.4 mV/m. The peak value of the electrostatic field measured directly by installing an electric field sensor at the bottom of the wave glider is relatively large. This is partly due to the shallow depth of the seawater and partly due to the bare metal leakage at the bottom of the glider; the induced electric field generated is relatively large.

Table 1. Summary of electric field characteristics in different motion states.

Status Number	Peak to Peak Value of Electrostatic Field (mV/m)	Peak to Peak Value of Shaft-Rate Electric Field (mV/m)	Hz Signal PSD (Power Spectral Density)	0.5~1 Hz Signal PSD (Power Spectral Density)
1	0.2	0.2~0.3	0.003	0.016
2	0.2	0.5	0.002	0.04
3	0.2~0.3	0.6~0.7	0.0025	0.045
4	0.3~0.4	0.8	0.05	0.08
5	0.2~0.3	0.6~0.7	0.005	0.07
6	0.14	0.2	0.008	0.0045

In summary, to reduce the peak value of the static electric field of the wave glider, it is possible to consider changing the distance between the underwater towed body and the surface parent body, as well as changing the metal structure of the towed body. To reduce the axial frequency electric field, the connection between the floating body on the water surface and the underwater towed body can be changed to reduce the significant change in direction, thereby reducing the change in rudder angle of the towed body and reducing the amplitude of the axial frequency electric field. According to the power spectrum analysis, it can be seen that the interference electric field generated during the motion of the wave glider is mainly concentrated within 1.5 Hz, and for some of the underwater moving bodies, the frequency of the axial-frequency electric field signals is concentrated in the range of 0.5–30 Hz, so that the use of the axial-frequency electric field of the underwater moving bodies can be considered to be detected.

4. Analysis of Magnetic Field Noise Characteristics

4.1. Measuring Principle

Due to the large shaking of the floating body on the water surface, installing a magnetic field sensor (magnetic sensors use three-axis flux gate sensors) on the upper part of the underwater tractor (as shown in Figure 11) will mainly be affected by two aspects of magnetic field interference: first, the tractor steering engine will continuously adjust the rudder angle underwater to maintain the heading, which will generate a magnetic field due to rotation and underwater traction machines generate strong shaking-related magnetic field noise.

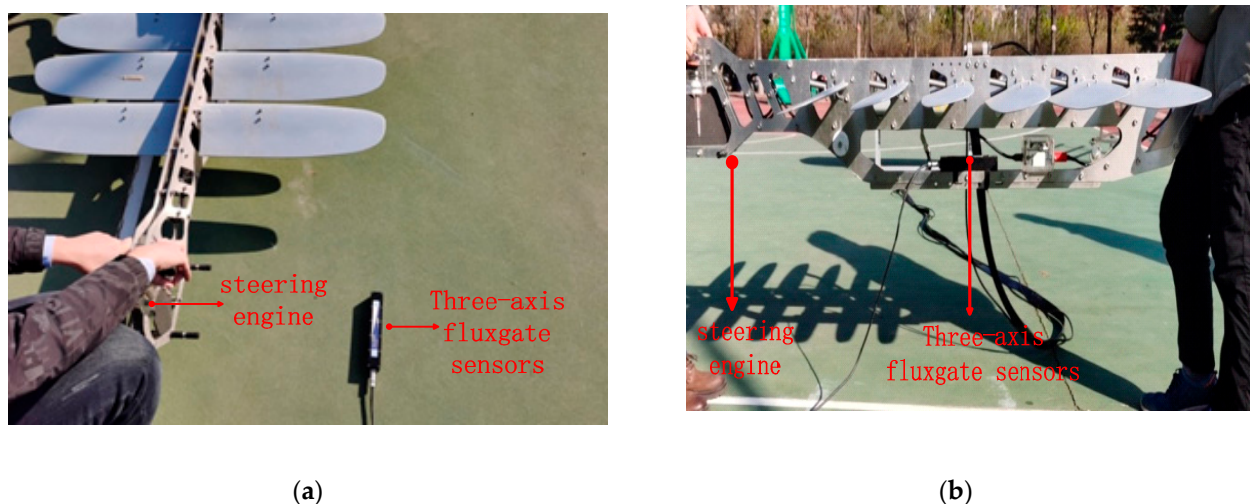


Figure 11. Measurement method for magnetic field of underwater gliders. (a) Measurement method for magnetic field of underwater towed steering engines. (b) Measurement method for magnetic field of underwater towed body shaking.

Firstly, place the three-axis flux gate sensor directly below the underwater towing machine. As the movement of the towing machine's steering engine motor must be caused by changes in its attitude angle, after the wave glider is powered on, control the steering engine motor's operation by changing its attitude angle to test the magnetic field generated by the steering engine motor.

For the induced magnetism generated by the motion of the underwater towing body itself, the testing personnel use the underwater towing body to pass directly above the magnetic sensor and artificially increase the shaking of the towing body during the process, simulating the real motion situation.

4.2. Measurement Result Analysis

Place the magnetic field sensor 30 cm directly below the steering engine for measurement, the measurement results are shown in Figure 12. As the action of the steering engine must be caused by changes in the angle of the tractor, the significant increase or decrease in the magnetic field in the figure is due to changes in the position of the tractor, while the rapid change in the magnetic field is caused by the action of the steering engine.

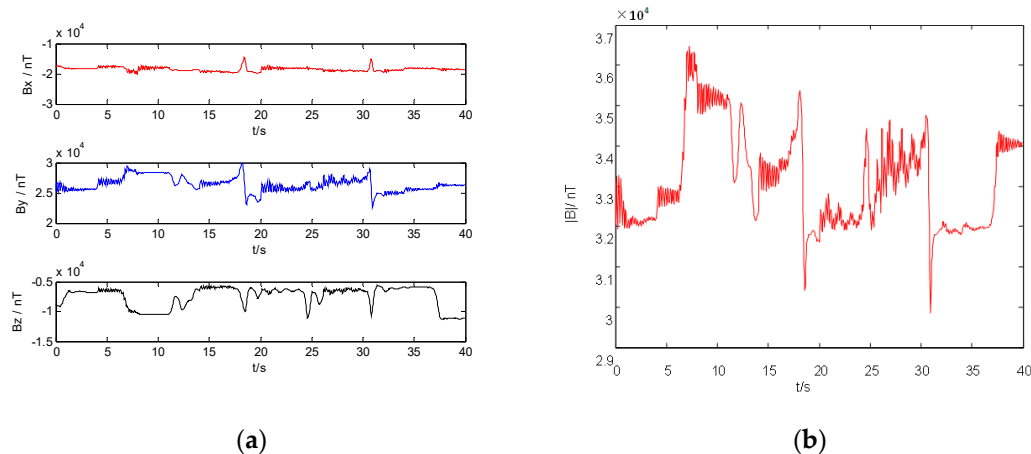


Figure 12. The magnetic field generated by the action of the underwater towing steering engine (sensor located directly below, with a distance of 30 cm). (a) Three-axis magnetic component; (b) magnetic modulus.

As can be seen from Figure 13, when the magnetic field sensor is mounted on the metal at the bottom of the traction machine, although there is a certain distance from the rudder, it will still be affected by the magnetic field interference generated by the rudder action. However, the amplitude is much smaller than that mounted directly below the rudder, which is due to the fact that the magnetic field signal is inversely proportional to the distance third power.

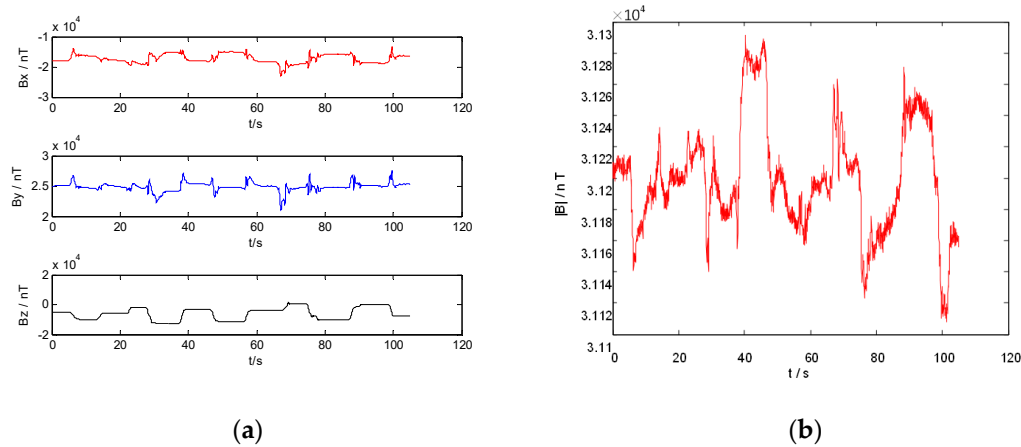


Figure 13. The magnetic field generated by the action of the underwater towing steering engine (sensors installed on metal trailers). (a) Three-axis magnetic component; (b) magnetic modulus.

As can be seen from the analysis in Figure 14, in order to simulate the magnetic field generated when the tractor is swaying under the action of waves, the peak value of the magnetic field associated with the swaying is measured to be about 20 nT when the sensor is placed at a location 80 cm directly below the tractor, and the magnetic field generated by the swaying is relatively stable with a small range of variation in the amplitude of the signal, unlike that caused by the rudder operation.

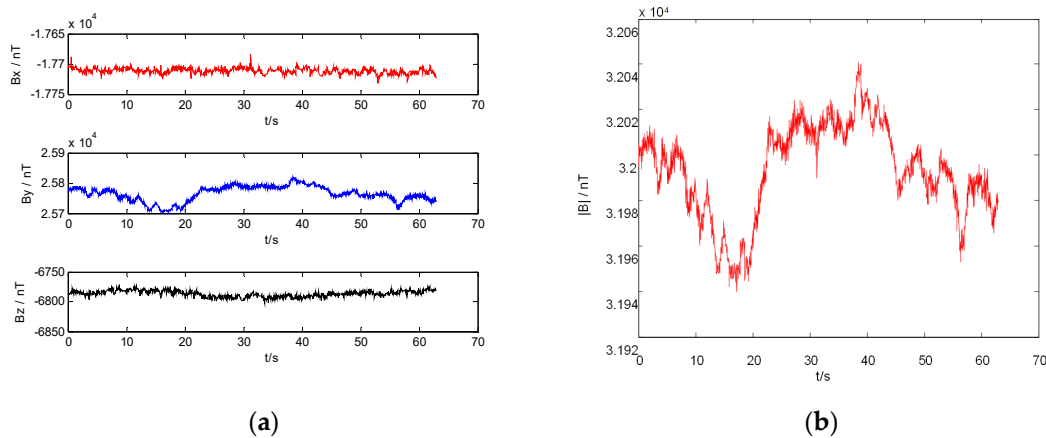


Figure 14. The sensor is located 80 cm directly below the tractor (the tractor shakes left and right, while the steering engine does not move). (a) Three-axis magnetic component; (b) magnetic modulus.

By analyzing the measurement results (as shown in Figure 15), it can be concluded that the sensor is located 80 cm directly below the underwater tractor, and the operation of the steering engine will still produce a certain impact on magnetic field measurement.

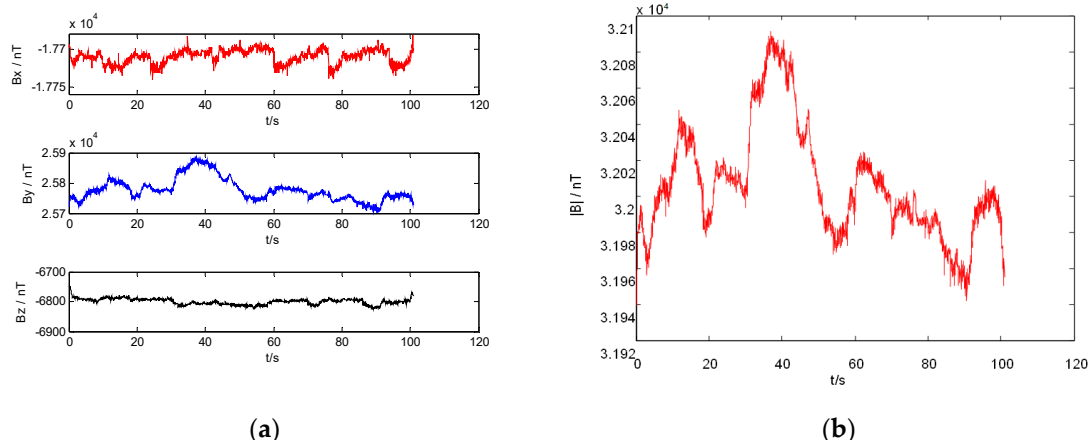


Figure 15. The sensor is located 80 cm directly below the tractor (underwater towing steering engine action). (a) Three-axis magnetic component; (b) magnetic modulus.

Measure the magnetic field intensity of the glider underwater towing machine (as shown in Figure 16), and the peak-to-peak value of the magnetic field when passing is about 80 nT. Due to the length of the towing machine being about 2 m, the magnetic moment of the towing machine is roughly calculated to be about $0.5 \text{ A} \cdot \text{m}^2$.

According to the analysis of the measured magnetic field data, it can be seen that the amplitude of the magnetic field signal generated by the underwater towing body swaying of the wave glider is small, and the change is relatively smooth, while the amplitude of the magnetic field signal generated by the rudder work is large and the speed of change is fast, so it can be known that the underwater towing body rudder is the main source of the magnetic field interference when the wave glider is underwater.

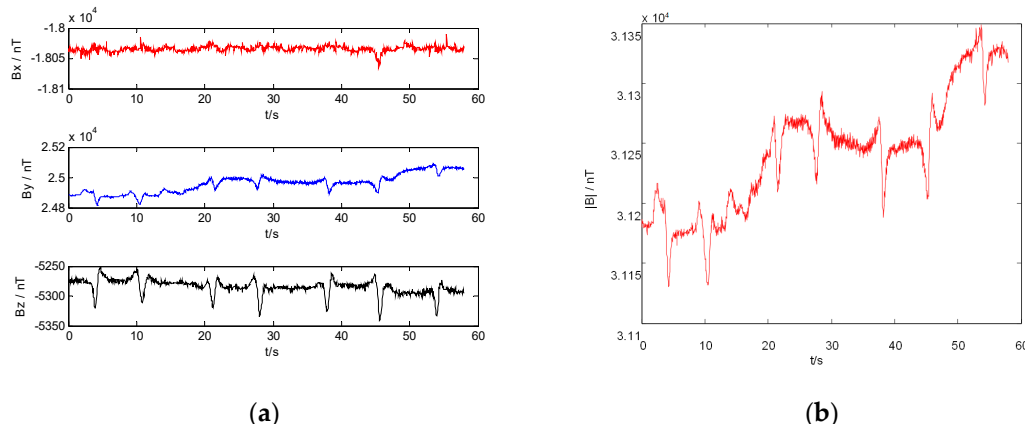


Figure 16. Magnetic field passing characteristics of underwater towing body (magnetic field 80 cm directly below, horizontal distance = 0 cm). (a) Three-axis magnetic component; (b) magnetic modulus.

5. Conclusions

When the wave glider works, its electromagnetic field interference is relatively large. The peak value of the axial frequency electric field is basically between 0.5 and 0.7 mV/m, the peak value of the electrostatic field is about 0.2~0.4 mV/m, the peak value of the magnetic field is about 80 nT, and the magnetic moment is about 0.5 A·m². Compared to the electromagnetic interference generated by the wobbling, the rudder works with a greater electromagnetic field interference.

Therefore, the electromagnetic sensor is restricted by the working conditions of the wave glider and is not suitable for direct installation. From the practical engineering point of view, in order to reduce the electromagnetic interference of the wave glider itself, the following methods can be considered: ① change the connection between the surface floating body and the underwater towing body to reduce the transmission of the swaying and rudder work amplitude; ② change the structure of the underwater towing body material, e.g., replace it with a non-metallic material to reduce the relevant section corrosion electric and magnetic fields; ③ design the equipment pods to hang the electromagnetic sensors in the deep-water area, which can interfere with the background environment and increase the stability of electromagnetic sensor operation; ④ change the rudder material and structure, consider the use of non-magnetic materials, or other directional adjustment devices to control the main electromagnetic field signals. Determining how to use wave gliders for underwater electromagnetic detection targeting will be the focus of future research.

Author Contributions: Data curation, T.X.; formal analysis, J.Z. and D.X.; investigation, D.X.; methodology, J.Z., D.X., T.X. and Q.J.; writing—original draft, J.Z.; writing—review and editing, T.X. and Q.J. All authors have read and agreed to the published version of the manuscript.

Funding: Supported by the Youth Fund of the National Natural Science Foundation of China (51509252).

Institutional Review Board Statement: Not applicable.

Informed Consent Statement: Not applicable.

Data Availability Statement: The data presented in this study are available upon request from the corresponding author.

Conflicts of Interest: The authors declare no conflict of interest.

References

- Wang, Y.; Liu, D.; Yang, Y. Summary of the Development of Unmanned Undersea Systems in 2019. *Unmanned Syst. Technol.* **2020**, *3*, 55–59. (In Chinese)
- Wang, Y.; Liu, D.; Yang, Y. Summary of the Development of Unmanned Undersea Systems in 2018. *Unmanned Syst. Technol.* **2019**, *2*, 20–25. (In Chinese)

3. Liu, Y.; Zhou, J.; Wang, X.; Zuo, M. Application of unmanned underwater vehicle in underwater offensive and defensive operations. *J. Nav. Univ. Eng.* **2021**, *18*, 84–88. (In Chinese)
4. Xiang, Q.; He, X. Research on Submarine Searching Method of Unmanned Marine Vehicle with Magnetic Anomaly Detector. *J. Ordnance Equip. Eng.* **2019**, *40*, 16–19. (In Chinese)
5. Liu, Z.; Wu, J.; Huang, F.; Du, Y. Compatibility Analysis of UUV Navigation System Based on Mission Classification. *J. Ordnance Equip. Eng.* **2019**, *40*, 82–86. (In Chinese)
6. Zhang, S.; Yu, D.; Sang, H.; Sun, X.; Liu, F. A new hybrid path planning method for the sailboat architecture wave glider in the wind field environment. *Ocean Eng.* **2023**, *283*, 115153. [[CrossRef](#)]
7. Liu, F.; Lan, T.; Wei, Z.; Sun, X.; Zhang, S.; Sang, H.; Huang, F. Adaptive propeller rudder controller for the wave glider with a propeller-rudder control system. *Ocean Eng.* **2023**, *289*, 116129. [[CrossRef](#)]
8. Yu, P.; Sun, X.; Zhou, Y.; Sang, H.; Zhang, S. Adaptive station-keeping strategy for wave gliders considering uncertain environmental disturbances. *Ocean Eng.* **2023**, *277*, 114326. [[CrossRef](#)]
9. Ma, X.; Wang, Y.; Li, S.; Niu, W.; Ma, W.; Luo, C.; Yang, S. Formation control of discrete-time nonlinear multi-glider systems for both leader-follower and no-leader scenarios under switching topology: Cases for a fleet consisting of a wave glider and multiple underwater gliders. *Ocean Eng.* **2023**, *276*, 114003. [[CrossRef](#)]
10. Xie, S.; Zumberge, M.; Sasagawa, G.; Voytenko, D. Shallow Water Seafloor Geodesy With Wave Glider-Based GNSS-Acoustic Surveying of a Single Transponder. *Earth Space Sci.* **2023**, *10*, e2023EA003043. [[CrossRef](#)]
11. Lyu, Z.; Wang, C.; Sun, X.; Zhou, Y.; Ni, X.; Yu, P. Real-time ship detection system for wave glider based on YOLOv5s-lite-CBAM model. *Appl. Ocean Res.* **2024**, *144*, 103833. [[CrossRef](#)]
12. Premus, V.E.; Abbot, P.A.; Kmelnitsky, V.; Gedney, C.J.; Abbot, T.A. A wave glider-based, towed hydrophone array system for autonomous, real-time, passive acoustic marine mammal monitoring. *J. Acoust. Soc. Am.* **2022**, *152*, 1814. [[CrossRef](#)]
13. Cheyne, H.A.; Hawthorne, D.; Key, C.R.; Satter, M.J. Near real-time detection, beam-forming, and telemetry of marine mammal acoustic data on a wave glider autonomous vehicle. *J. Acoust. Soc. Am.* **2014**, *135*, 2336. [[CrossRef](#)]
14. Cheyne, H.A.; Key, C.R.; Satter, M.J. Detection, bearing estimation, and telemetry of North Atlantic right whale vocalizations using a wave glider autonomous vehicle. *J. Acoust. Soc. Am.* **2014**, *136*, 2117. [[CrossRef](#)]
15. Cimino, M.; Cassen, M.; Merrifield, S.; Terrill, E. Detection efficiency of acoustic biotelemetry sensors on Wave Gliders. *Anim. Biotelemetry* **2018**, *6*, 16. [[CrossRef](#)]
16. Ko, S.H.; Hyeon, J.W.; Lee, S.; Lee, J.H. Observation of Surface Water Temperature and Wave Height along the Coast of Pohang using Wave Gliders. *J. Coast. Res.* **2018**, *85*, 1211–1215. [[CrossRef](#)]
17. Cheng, J.; Zhang, J.; Jiang, R. Development status of underwater electromagnetic detection technology. *Digit. Ocean Underw. Warf.* **2019**, *2*, 45–49. (In Chinese)
18. Zhao, W.; Jiang, R.; Yu, P.; Zhang, J. Detection and identification of ship shaft-rate electric field based on line-spectrum characteristics. *Acta Armamentarii* **2020**, *41*, 1165–1171. (In Chinese)
19. Birsan, M. Measurement of the extremely low frequency (ELF) magnetic field emission from a ship. *Meas. Sci. Technol.* **2011**, *22*, 085709. [[CrossRef](#)]
20. Lin, C.; Gong, S. *Warship Physical Field*, 2nd ed.; The Publishing House of Ordnance Industry: Beijing, China, 2007; pp. 25–256. (In Chinese)
21. Schaefer, D.; Doose, J.; Rennings, A.; Erni, D. Numerical Analysis of Propeller-induced Low-frequency Modulations in Underwater Electric Potential Signatures of Naval Vessels in the Context of Corrosion Protection Systems. Presented at the COMSOL Conference 2011, Boston, MA, USA, 26–28 October 2011.
22. Mu, J.; Liu, Y.; Li, P.; Zhu, K.; Wang, W. Design of an underwater rudder for a wave glider. *China's New Technol. Prod.* **2019**, *40*, 16–19. (In Chinese)
23. Zhang, W.; Liu, Y.; Ma, S. Research on Anti-Interference Nonlinear Adaptive Control Method for Autonomous Underwater Gliders. *J. Ordnance Equip. Eng.* **2021**, *42*, 165–169. (In Chinese) [[CrossRef](#)]
24. Li, X.; Wang, L.; Wu, X.; She, H. Principle and System Design of a Wave Glide. *J. Sichuan Ordnance* **2013**, *34*, 128–131. (In Chinese)
25. Tian, Y.; Wu, X.; Wang, H.; Xiong, T.; Wang, H.; Ban, W.; Wu, W. Research Progress and Development Thinking of "Sea Ray" Wave Glider. *Digit. Ocean Underw. Warf.* **2020**, *3*, 111–122. (In Chinese)

Disclaimer/Publisher's Note: The statements, opinions and data contained in all publications are solely those of the individual author(s) and contributor(s) and not of MDPI and/or the editor(s). MDPI and/or the editor(s) disclaim responsibility for any injury to people or property resulting from any ideas, methods, instructions or products referred to in the content.